
# Vibrational relaxation as the driving force for wavelength conversion in the peridinin-chlorophyll a-protein

Jan P. Götze, Bora Karasulu, Mahendra Patil, Walter Thiel

PII: S0005-2728(15)00154-1
DOI: doi: 10.1016/j.bbabio.2015.07.011
Reference: BBABIO 47508

To appear in: *BBA - Bioenergetics*

Please cite this article as: Jan P. Götze, Bora Karasulu, Mahendra Patil, Walter Thiel, Vibrational relaxation as the driving force for wavelength conversion in the peridinin-chlorophyll a-protein, *BBA - Bioenergetics* (2015), doi: 10.1016/j.bbabio.2015.07.011

# Vibrational relaxation as the driving force for wavelength conversion in the peridinin-chlorophyll a-protein

Jan P. Götze*[,†], Bora Karasulu[‡], Mahendra Patil[§] and Walter Thiel[‡]

[†]School of Chemistry, North Haugh, University of St Andrews, St Andrews, Fife KY16 9ST, UK
E-Mail: jpg9@st-andrews.ac.uk
Phone: +(44)(0)1334-46-4748 (ext. 14141)
Fax: +(44)(0)1334-46-3808
[‡]Max-Planck-Institut für Kohlenforschung, Kaiser-Wilhelm-Platz 1, D-45470 Mülheim an der Ruhr, Germany
[§]Center for Excellence in Basic Sciences, University of Mumbai, Mumbai 400098, Maharashtra, India

**Abstract**

We present a computationally derived energy transfer model for the peridinin-chlorophyll a-protein (PCP), which invokes vibrational relaxation in the two lowest singlet excited states rather than internal conversion between them. The model allows an understanding of the photoinduced processes without assuming further electronic states or a dependence of the $2A_g$ state character on the vibrational sub-state. We report molecular dynamics simulations (CHARMM22 force field) and quantum mechanics/molecular mechanics (QM/MM) calculations on PCP. In the latter, the QM region containing a single peridinin (Per) chromophore or a Per-Chl *a* (chlorophyll a) pair is treated by density functional theory (DFT, CAM-B3LYP) for geometries and by DFT-based multireference configuration interaction (DFT/MRCI) for excitation energies.

The calculations show that Per has a bright, green light absorbing $2A_g$ state, in addition to the blue light absorbing $1B_u$ state found in other carotenoids. Both states undergo a strong energy lowering upon relaxation, leading to emission in the red, while absorbing in the blue or green. The orientation of their transition dipole moments indicates that both states are capable of excited-state energy transfer to Chl *a*, without preference for either $1B_u$ or $2A_g$ as donor state. We propose that the commonly postulated partial intramolecular charge transfer (ICT) character of a donating Per state can be assigned to the relaxed $1B_u$ state, which takes on ICT character. By assuming that both $1B_u$ and $2A_g$ are able to donate to the Chl *a* Q band, one can explain why different chlorophyll species in PCP exhibit different acceptor capabilities.

## Introduction

The peridinin-chlorophyll a-protein, PCP,[a] is a water soluble light harvesting protein found in dinoflagellates.[1] In contrast to most other, often membrane-bound light harvesting complexes, PCP exhibits an orange color, indicating absorption in the blue and green ranges of the solar spectrum,[2] caused by a structurally complex carotenoid, peridinin (Per).[3] There are eight Per molecules in the main form of the PCP protein complex that surround only two chlorophyll (Chl) *a* in sets of four Per each, leading to pseudo-$C_2$ symmetry in PCP.[4] In a high-salt variant, six Per are found instead of eight.[5] In other light harvesting proteins and complexes, carotenoids act as a supporting element and not as the main light harvesting chromophore.[6]

Because of its absorption spectrum and molecular composition, PCP has attracted much attention in the past.[4, 7] The unusual color of the protein is due to the intense harvesting of photons from the blue to green region of the solar spectrum, including the "green gap", which gives nearly all plants their characteristic appearance. Due to the low Chl *a* amount, almost no light from the red or yellow regions is harvested, leading to the characteristic orange color (see Figure 1 for an experimental spectrum of PCP). This allows the dinoflagellates to harvest light that passes through other photosynthetic organisms. Experimentally, PCP exhibits high, near-100% energy transfer efficiency from the main chromophore Per to Chl *a*.[2a, 8] Several pathways have been proposed for this energy transfer, as summarized in a recent review.[9]

Based on simple π-electron methods and group theoretical considerations, linear polyenes like carotenoids should exhibit in the UV/vis region a series of optically bright and dark singlet states, which can be labeled in an idealized $C_{2h}$ symmetry as: $1A_g$ ($S_0$, ground state), $2A_g$ ($S_1$, dark), $1B_u$ ($S_2$, bright), and $2B_u$ ($S_3$, dark).[10] The exact order of these states depends on the length of the linear polyene in question.[11] However, for the carotenoids involving a β-carotene-like chain length, the order of states listed above has been repeatedly found in theory and experiment.[11-12]

It is well established that Chl *a* $Q_y$ is the state responsible for the energy feed to the photosynthetic reaction center,[6] requiring an excited-state energy transfer (EET) from Per to Chl *a* beforehand. With Per as the dominant absorbing chromophore, the core question about PCP is how the initially absorbed energy (about 400-500 nm, blue-green region) is tuned down to the

[a] List of important abbreviations, alphabetical order: BLA - bond length alternation; Chl - Chlorophyll; CPCM - Conductor polarization continuum model; EET - Excitation energy transfer; HOMO - Highest occupied molecular orbital; IC - Internal conversion; ICT - Intramolecular charge transfer; LE - Local excitation; LUMO - Lowest unoccupied molecular orbital; MD - molecular dynamics; MRCI - Multireference configuration interaction; PCP - Peridinin–chlorophyll *a*–protein; Per - Peridinin; QM/MM - Quantum mechanics/molecular mechanics; TD–DFT - (Time–dependent–) Density functional theory; VR - Vibrational relaxation

spectral region of the Chl *a* Q-band (600 nm and below). Femtosecond transient absorption spectroscopy shows that this process involves the formation of an internal charge transfer (ICT) state with a lifetime of 2-3 ps that transfers energy quantitatively into Chl.[13] Several pathways for the formation of the ICT state have been proposed, most of them involving internal conversion (IC) as the basic mechanism;[9] a recent study has provided experimental and theoretical evidence for the direct formation of the ICT state by $1B_u/2A_g$ state mixing along the $1B_u$ relaxation path.[12f]

Computational modeling can address these issues through an explicit analysis of the excited states and the photoinduced processes. However, theoretical studies have struggled with carotenoids in the last decade because certain important excited states cannot be modeled properly using the computationally efficient time-dependent density functional theory (TD-DFT).[14] Problems arise for states that contain a significant amount of multi-electron excitation character, i.e. for about every second electronic state of Per in the UV/vis region.[12c, 15] Much effort was invested to develop and evaluate methods that allow for a reliable description of these states.[11, 12e, 12f, 16]

In computational work on polyenes, there are some methodological caveats. For carotenoids, a proper calculation of the bond length alternation (BLA) is crucial, a feature that has been shown to strongly affect the vertical spectra even at small degrees of BLA deviation for linear polyenes.[12d, 17] Semiempirical approaches may be the method of choice for large-scale studies with whole sets of chromophores.[16e, 18] However, it remains to be seen if the semiempirical BLA values of excited-state geometries are robust when compared to other methods such as DFT.[16f, 17a, 17c] For carotenoids, the choice of the method used during geometry optimization is thus not trivial, and different choices may yield different photophysics.[12e, 12f, 16f-h]

Recently, we have proposed that the description of carotenoid function may be incomplete without including the Soret band of chlorophylls.[17d] We were able to distinguish between the role of two carotenoid compounds on the basis of a vibrational relaxation model for the $1B_u$ state. However, in PCP, Per is the dominant component, and the Soret band of Chl *a* should only play a minor role in the actual absorption spectrum. We also found previously that the $1B_u$ state in other carotenoids can relax from the blue absorbing region into a red fluorescence region.[12d] For a compound like Per, the main light harvester in PCP, this process might be important and could explain several of the experimental findings. A recent ab initio study on Per in various polar solvents (represented by the polarizable continuum model, PCM) has indeed shown that geometry relaxation in the excited state is relevant and strongly affects the nature of the ICT state of the carotenoid.[12f] One may thus suspect similar behavior for Per in PCP.

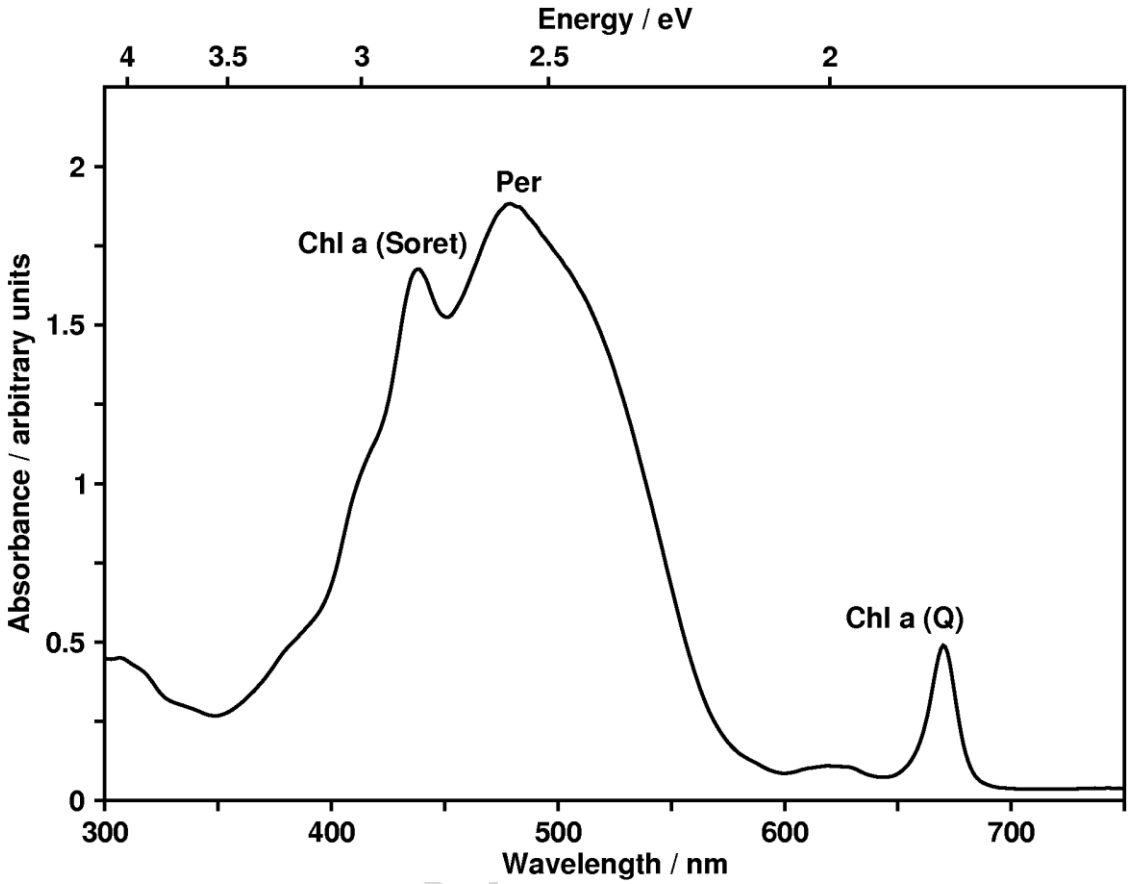


**Figure 1**. Experimental spectrum of PCP in water. Data kindly provided by Dr. Heiko Lokstein, Glasgow.

In previous studies,[17c, 17d] we employed a scheme that tested the role of the protein environment by activation/deactivation of the corresponding Coulombic representation in the form of a point charge field. We continue to use this scheme here, but augment it by quantum mechanics/molecular mechanics (QM/MM).[19] We perform force field molecular dynamics (MD) simulations followed by a series of snapshot QM/MM calculations (see below). Using this scheme, we can include some structural sampling due to the preceding MD procedure. We should thus be able to get an impression on how much the flexibility of the protein influences the excitation energies, the oscillator strengths, and the relative orientations of transition dipole moments.

## Methods

For the initial geometry setup, a PCP monomer of *Amphidinium carterae* from the protein data bank (PDB ID: 1PPR[4]) was solvated in a water ball of 30 Å radius, preserving the positions of the crystal waters and neutralizing the overall positive protein charge with $Cl^-$ ions. The missing hydrogen atoms were added using CHARMM[20] or manually in the case of the frozen residues (see below). After an initial energy minimization using the adopted basis Newton-Raphson scheme (80 steps) MD simulations were performed with CHARMM, during which the borders of the system were constrained by spherical boundary conditions, and hydrogen atoms were kept at their respective equilibrium bond distances using the SHAKE algorithm.[21] The system was prepared with a 1 fs time step for 25 ps by stepwise heating/equilibration to 300 K. The following production run lasted for 250 ps in an NVT setup. The system was coupled to a Nose-Hoover thermostat at 300 K.[22] The MD methodology was in most aspects identical to the one described in detail in a previous study.[23]

In the above calculations, we had to cope with the lack of reliable, tested parameters for parts of the system, namely the chromophores and the lipids in PCP. Hence, we decided to study only the influence of solvent and amino acids dynamics, in analogy to our previous studies.[17c, 17d] The lipid, Per, and Chl *a* molecules were thus frozen during MM optimizations and MD runs. The remaining non-bonding interactions were represented by standard CHARMM[20] van-der-Waals parameters and by Merz-Kollmann[24] charges calculated from B3LYP[25] with a 6-311G* basis set.[26] The hydrogen positions of the frozen compounds were optimized before the MD simulations using the semiempirical MNDO method.[27]

For five selected MD snapshots, QM/MM optimizations were conducted using the Gaussian09 software[28] interfaced with DL_POLY[29] via ChemShell.[19a] The QM part consisted of a single Per molecule (PID614, see Figure 2) and was

described by the CAM-B3LYP[30] functional with a 6-31G(d) basis.[26] The active region in the QM/MM optimizations included all residues within 10 Å around PID614, applying the same restrictions for the MM residues without available force field parameters as indicated above for the MD runs. For one snapshot, we additionally included a Chl *a* and a water molecule (CLA601 and HOH701, see Figure 2) in the QM part to obtain a corresponding spectrum; we decided to limit the testing to this one case in view of our previous experience that chlorophyll state energies and oscillator strengths are rather insensitive to the Chl *a* geometry.[17c, 17d] Results from analogous calculations with a B3LYP[25] rather than a CAM-B3LYP treatment of the QM region can be found in the Supporting Information (SI).

For comparative purposes, the two chromophores were also optimized in the gas phase or with an implicit solvent model (CPCM[31]), and the corresponding excited states were computed for these geometries as well using TD-DFT and DFT/MRCI with an implicit solvent model (for TURBOMOLE: COSMO[32]).

TD-DFT[14] calculations were run at the QM/MM optimized structures to obtain linear-response excited-state results. To access the states unavailable with TD-DFT, we computed vertical singlet excitation energies with a combined DFT and MRCI approach (DFT/MRCI[33]) at the same geometries. For DFT/MRCI, the orbitals were generated using TURBOMOLE,[34] the BHLYP[35] functional and the SVP basis.[36] The SVP basis was previously shown to work well for the state energies of carotenoid systems at significantly lower cost compared to a TZVP basis.[11] The point charges of the MM part were either active or inactive during the DFT/MRCI calculations at the QM/MM geometries, allowing the analysis of electronic embedding effects on the excitations.[17c, 17d]

Finally, we relaxed the $1B_u$ state at the TD-DFT level. To reduce the required effort for the excited-state optimizations, these calculations were done in the gas phase. We consider this to be justified, as long as we are looking for a qualitative assessment of the relaxation energy in the $1B_u$ state. Furthermore, our previous studies with other carotenoids indicate that the environmental influence on geometries is limited and relevant only in some situations, such as state crossings. Indeed, the choice of density functional (e.g., CAM-B3LYP vs. B3LYP) appears to affect the geometry more strongly than the environment (see the B3LYP results in the SI). We did not optimize the $2A_g$ state, since this is not possible in the framework of the chosen CAM-B3LYP methodology. While we mainly focus on the $1B_u$ state in this work, we will use the insight provided by another study by Knecht, Marian, Kongsted and Mennucci[16f] to support our model with the parts of the picture that involve the $2A_g$ state.

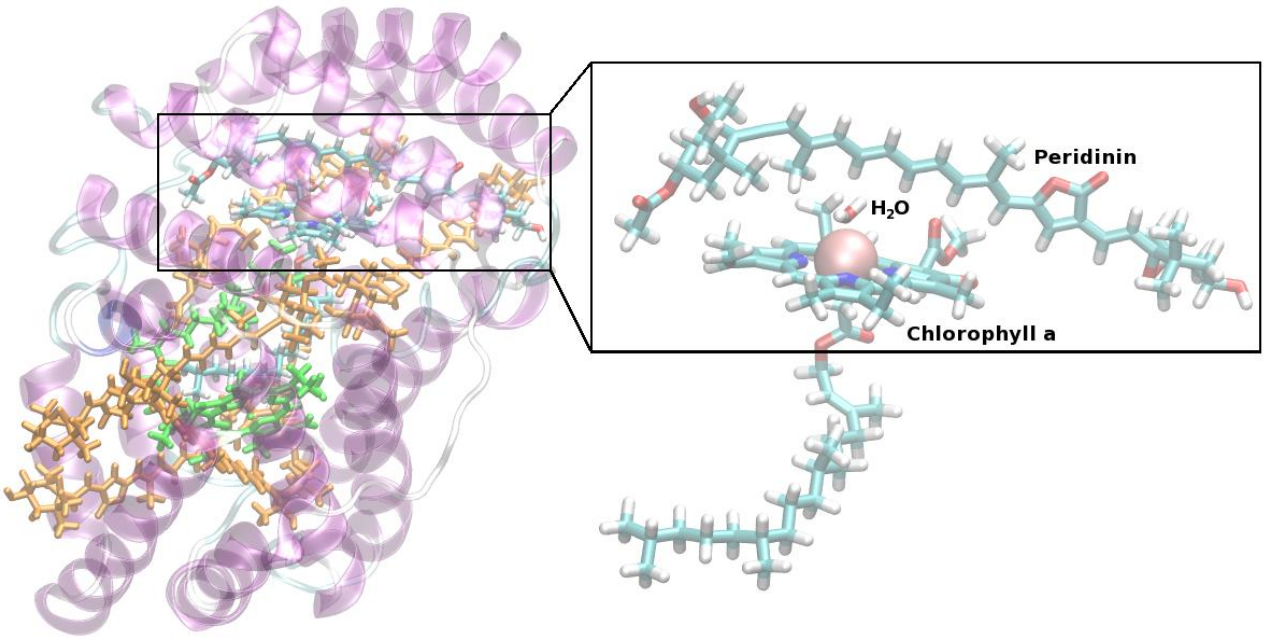


**Figure 2.** Location of the chromophores of interest (CLA601, PID614) and of the Mg-coordinating crystal water molecule (HOH701) in the PCP complex from *Amphidinium carterae* (PDB ID: 1PPR).[4] The right-hand side shows the QM/MM optimized chromophores (see text for details). Other Chl *a* and Per species are drawn in green or orange, respectively.

## Results

(a) Peridinin bond length alternation

As the linear polyene part of Per is the dominating structural element for the optical spectrum, a BLA analysis is in order (Figure 3). The BLA strongly affects the relative state energies (excitation/fluorescence energies), as well as the corresponding state character and composition.[12e, 16f] As such, the BLA allows us to link changes in geometry to changes in the spectrum. We define the BLA as

$$BLA_n = (-1)^{n+1} (r_n - r_{n+1}) \quad (1)$$

with $r_n$ being the length of bond n as indicated in Figure 3. This definition is identical to the one given by Kleinschmidt et al.[11] We find that Per, despite the presence of the lactone ring, displays a BLA pattern similar to that of β-carotene up to n=11. This is remarkable, as one might expect an influence of the structural differences. However, it appears that Per features the BLA of a

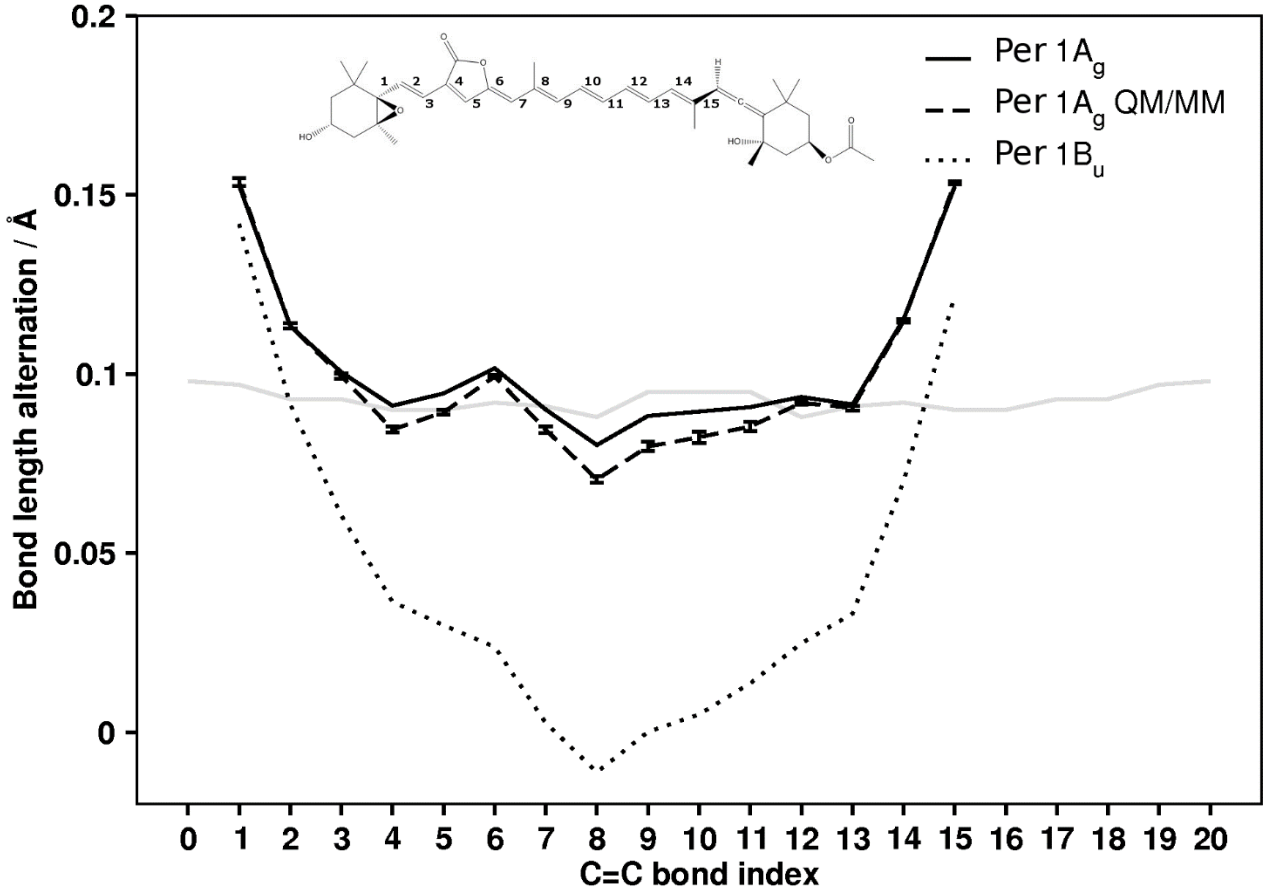


**Figure 3.** Bond length alternation (BLA) along the conjugated chain of Per in the $1A_g$ (solid line: gas phase, dashed line: QM/MM) and $1B_u$ states (dotted line). Vertical bars indicate the standard deviation between QM/MM snapshots. The crystal β-carotene BLA (grey, solid line) derived from structural data obtained by Senge et al.[37] is included as a reference for comparison to larger carotenoids.

longer carotenoid on the lactone-containing side, without actually providing the same overall conjugated chain length. The BLA was shown to be decisive for the absorption to $2A_g$ and $1B_u$.[16f]

Introducing the protein/solvent at the QM/MM level results in overall lower BLA values (Figure 3, dashed line), with negligible variations between the different snapshots (vertical bars on dashed line). Due to this slight drop in BLA, one would expect to compute a slightly red-shifted absorption spectrum in PCP compared to the gas phase. This relation between BLA and absorption energies has been established previously for Per[16f] and other carotenoids as well.[11, 12d]

The excited-state geometries of Per in various solvents have been computed at the CIS[8,8] level (configuration interaction with single excitations in an [8,8] active space) using the PCM solvent model.[12f] We note that the excited-state BLA from these calculations[12f] is less pronounced than that found in our CAM-B3LYP optimizations (for example, in methanol by about 0.05 Å, data not shown), which may lead to qualitative differences in the resulting transition energies (see below). Comparisons for the ground-state gas-phase structures obtained from various DFT, Hartree-Fock, and high-level variational Monte Carlo (VMC) methods indicate that CAM-B3LYP performs most closely to VMC, with Hartree-Fock showing a slightly higher and CAM-B3LYP a slightly lower BLA than VMC.[16h]

(b) Peridinin and chlorophyll *a* vertical energies

The computed vertical excitation/fluorescence energies of Per and Chl *a* allow us to understand the energy range, in which the photophysics is likely to happen. Vertical energies can be considered as extremes, as excitation (fluorescence) maxima are likely to be found at lower (higher) energies than the vertical energies.[12d] Comparing the values from different methods provides an estimate of their reliability (see for example a recent evaluation on the basis of B3LYP geometries[16g]).

Our computed TD-DFT and DFT/MRCI vertical excitations are given in Table 1. The results from both methods differ to some extent, consistent with the trends observed in previous studies.[11, 12d, 16f, 17d] Generally, CAM-B3LYP excitation energies are higher than those from DFT/MRCI (and B3LYP, see SI). Note that the order of DFT/MRCI states is adapted to TD-DFT by comparing the contributing orbitals (TD-DFT) or determinants (DFT/MRCI), which leads to the DFT/MRCI Soret1 state to be higher in energy than DFT/MRCI Soret2 state. Our gas-phase B3LYP+DFT/MRCI Per vertical excitation energies agree with the results from Knecht et al.[16f] within 0.02 eV or less (see SI for a more detailed comparison). Taking our previous experience with other xanthophyll

compounds into account, we consider CAM-B3LYP to be more reliable for the calculation of excited-state properties than B3LYP,[12d] and hence we focus our analysis on the CAM-B3LYP structures.

Due to the limitations of TD-DFT regarding the $2A_g$ state (see above), we will first restrict our analysis to the $1A_g$ and $1B_u$ states. We will later on complete the picture of the PCP pathway using the insights from Knecht et al.,[16f] Bricker and Lo[16e] and some of our own results on $2A_g$.

The results for Per in Table 1 show that the acetone environment introduces a red shift in $\Delta E_v$ of -0.19 eV in the case of TD-DFT compared to the gas phase. For DFT/MRCI, the $\Delta E_v$ shifts are much smaller (less than -0.05 eV) indicating that $1B_u$ is less responsive to a polar environment when described with DFT/MRCI compared to TD-DFT. The corresponding DFT/MRCI shift for going from the gas phase to acetonitrile is -0.09 eV at B3LYP geometries as reported elsewhere.[16f] We agree with the assessment that the third excited state of Per ($2B_u$) is well above the $1B_u$ state, regardless of the geometry.[16f] This is different from other carotenoids, where there might even be a $1B_u/2B_u$ crossing that is sensible to the solvent environment.[12d] Small solvent-induced red shifts in the two lowest vertical excitation energies of Per have also been found in equation-of-motion-coupled-cluster-singles-and-doubles (EOM-CCSD) calculations at CIS[8,8] excited-state geometries; it should be noted, however, that the gas-phase EOM-CCSD//CIS values are strongly blue-shifted (by about 0.7 eV) relative to our DFT/MRCI//CAM-B3LYP values.[12e, 12f]

For Chl *a*, the largest effect of the acetone environment is seen for the Soret band in TD-DFT, which is likely due to a nearby intermolecular Chl *a* charge transfer state mixing with the locally excited Soret1 and Soret2 states (data not shown). This does not occur at the DFT/MRCI level, where the effect of acetone on the Chl *a* $\Delta E_v$ is minute.

**Table 1. Vertical excitation energies ($\Delta E_v$, in eV) and oscillator strengths (f) obtained from TD-CAM-B3LYP or DFT/MRCI calculations for Chl *a* and Per, in the gas phase or with implicit solvent (acetone, for comparison to experiment) at the corresponding CAM-B3LYP geometries.**

| | Ground-state geometries | | | | | | | | Per $1B_u$ geometry | | | |
|---|---|---|---|---|---|---|---|---|---|---|---|---|
| | Gas Phase | | | | PCM (acetone) | | | | Gas Phase | | | |
| | TD-DFT | | DFT/MRCI | | TD-DFT | | DFT/MRCI | | TD-DFT | | DFT/MRCI | |
| | $\Delta E_v$ | f | $\Delta E_v$ | f | $\Delta E_v$ | f | $\Delta E_v$ | f | $\Delta E_v$ | f | $\Delta E_v$ | f |
| $Q_y$ | 2.18 | 0.21 | 1.96 | 0.25 | 2.14 | 0.32 | 1.95 | 0.27 | / | / | / | / |
| $Q_x$ | 2.51 | 0.04 | 2.14 | 0.03 | 2.49 | 0.10 | 2.12 | 0.05 | / | / | / | / |
| Soret1 | 3.45 | 0.70 | 3.03 | 0.52 | 3.35 | 0.93 | 2.99 | 0.42 | / | / | / | / |
| Soret2 | 3.68 | 0.93[a] | 3.02 | 0.44 | 3.57 | 1.10 | 2.98 | 0.39 | / | / | / | / |
| $2A_q$ | / | / | 2.52 | 1.12 | / | / | 2.50 | 1.69 | / | / | 1.81 | 0.01 |
| $1B_u$ | 2.89 | 3.49 | 2.77 | 2.22 | 2.70 | 3.53 | 2.74 | 1.66 | 2.30 | 3.71 | 2.31 | 3.34 |
| $2B_u$ | / | / | 3.37 | 0.02 | / | / | 3.38 | 0.00 | / | / | 2.70 | 0.00 |

[a] Lost some oscillator strength to a close intramolecular CT state, not shown

When looking at experimental spectra in acetone, the peak maxima of Chl *a* are located at 1.91 eV for the Q band and at 2.67 eV for the Soret band,[38] while PCP exhibits a broad experimental peak maximum around 2.6 eV.[8] The DFT/MRCI values are clearly much closer to experiment than those provided by CAM-B3LYP, yet still slightly blue shifted (0.05 eV for $Q_y$, 0.35 eV for Soret and about 0.1-0.2 eV for Per), as is to be expected when comparing vertical excitations to experimental band maxima.[12d]

For the Per $1B_u$ gas-phase minimum, we find that the vertical fluorescence energy of $1B_u$ is 0.46 eV lower than its vertical absorption energy. Such a large change was observed before for other carotenoids: Compared to violaxanthin (0.34 eV) or zeaxanthin (0.48 eV),[12d] the Per $1B_u$ relaxation energy is closer to that of the longer, β-carotene-like zeaxanthin. This indicates that although the Per π-chain is shorter compared to other carotenoids (see Figure 3), typical features are apparently conserved, such as the change in BLA discussed in the previous section. It appears that in Per, the shortening of the conjugated carbon chain by introducing the allyl group may be compensated by the presence of the lactone ring. In any case, it appears that the drop in energy within $1B_u$ is already bridging the gap between the blue and red spectral regions. Translated to wavelength units, the computed vertical absorption to and emission from $1B_u$ occurs at about 450 and 540 nm, respectively, with emission only slightly above the $Q_x$ region. This is consistent with an energy transfer pathway from $1B_u$ directly to Q, likely $Q_x$.[39]

The Per $2A_g$ state exhibits features different from those observed in other carotenoids. As already mentioned, detailed recent studies on the geometry dependence of the $2A_g$ results are available.[12e, 12f, 16f] Our calculations agree with the previous DFT/MRCI results,[19a] as we find $2A_g$ to share oscillator strength with $1B_u$ at the ground-state geometry (Table 1). This sharing of oscillator strength is less pronounced in the EOM-CCSD calculations,[12e, 12f] but very strong in many-body Green's functions calculations (where the energetically lower state dominates the spectrum).[16h] It has been linked to the BLA parameter and to the ratio of single/double excitation character,[16f] which is confirmed by our present data (not shown). It should be pointed out that our theoretical results are at odds with some experimentally derived models[9] for the energy transfer in PCP: Apparently, it is not the $S_2$ ($1B_u$) state that is shifted to lower wavelengths to facilitate the green absorption, but it is the $S_1$ ($2A_g$) state that is shifted up in energy. Considering light harvesting, closing the energy gap between $1B_u$ and $2A_g$ is counterproductive as it limits the available absorption wavelengths, and as such it is likely a price to be paid for the acquisition of $2A_g$ oscillator strength. This is also in conflict with models that regard $1B_u$ as the only absorbing Per state.[12f, 16b, 40] We will see however

in the course of this article that the theoretically derived model is sound and can explain several aspects of the PCP energy transfer pathway.

At this point, we should mention an MNDO/CAS-CI investigation of the properties of the $2A_g$ state of Per.[16e] Unfortunately, there are currently no benchmarks available that would support the suitability of this approach for the excited-state minimum geometries of linear polyenes. Comparing to the study of Knecht et al.,[16f] it appears that the semiempirical results[16e] are at the lower end or even below the predicted potential $2A_g$ emission range (1.6-2.4 eV). The MNDO/CAS-CI $1B_u$ geometries given in ref.[16e] yield a slightly lower overall BLA (by 0.02 Å, absolute values summed over the whole chain, data not shown) compared to our CAM-B3LYP geometries. Earlier studies have shown that quite small BLA differences can give rise to large differences in the absorption spectrum.[11, 12d, 16f] The CAM-B3LYP geometries apparently outperform even MP2 in terms of BLA[17a] and we are thus confident that our present approach provides a realistic picture.

(c) Dipole moments of Per states

A characteristic feature of PCP is that intramolecular charge transfer (ICT) precedes the associated energy transfer from Per to Chl *a*.[13, 41] The energy transfer arising from this channel is supposed to be slower than the one that involves a locally excited state.[42] We thus need to analyze the ICT character of the states to allow for an assignment of our proposed energy channels to experiment. In this study, we have introduced the protein environment explicitly, enabling us to see its effect on the Per and Chl *a* dipole moments. The PCP environment in PCP has been considered to be of moderate polarity,[9] which should be reflected by our model. The changes of the state dipole moments of Per are listed in Table 2 for various geometries and environments.

At the ground-state geometry, the transition to the $2A_g$ ($S_1$) state causes a strong change in the dipole moment of Per, i.e. an increase by 8.9/11.6 Debye in the gas phase/CPCM models, and by up to 18 Debye for the QM/MM models with electronic embedding. The dipole moment changes much less upon vertical excitation from the ground state to the $1B_u$ ($S_2$) state. Hence, it would be tempting to assume that the $2A_g$ state is the donor to the Chl *a* Q band because of its ICT character after vertical excitation. This would be a

**Table 2. DFT/MRCI dipole moments, in Debye. QM/MM geometries were optimized either without (gas) or with the PCP point charge field (PCF); average values over five snapshots are given with corresponding standard deviations. States with strong CT character are underlined.**

| | Ground-state geometries | | | | $1B_u$ geometry |
|---|---|---|---|---|---|
| | Gas phase | Acetone | QM/MM (gas) | QM/MM (PCF) | Gas phase |
| $1A_g$ | 3.52 | 5.02 | 2.68 ± 0.14 | 5.33 ± 0.46 | 3.31 |
| $2A_g$ | <u>12.46</u> | <u>16.58</u> | <u>10.87 ± 0.23</u> | <u>22.77 ± 1.09</u> | 2.48 |
| $1B_u$ | 4.19 | 5.40 | 3.40 ± 0.16 | 5.08 ± 0.43 | <u>13.12</u> |

premature conclusion, however, as the character of the lowest excited states changes upon geometry optimization.[12f] The mixing of ionic ($B_u$) and covalent ($A_g$) configurations[12f] is connected to the amount of BLA, as already shown for the DFT/MRCI case.[16f]

In the gas phase, at the TD-CAM-B3LYP $1B_u$ minimum geometry, it is not the $1A_g \rightarrow 2A_g$ transition that exhibits the largest change in dipole moment; it is the bright excitation of $1B_u$ ($S_2$). According to our computations, $1B_u$ starts as a locally excited (LE) state and ends up with ICT character after relaxation. In the EOM-CCSD and SAC-CI calculations by Wagner et al.,[12f] the lowest excited state of Per also acquires ICT character in polar solvents (PCM model) upon geometry optimization (CIS), accompanied by a $2A_g$ / $1B_u$ crossing during the relaxation from the Franck-Condon geometry. In the gas phase, there is no such crossing; in the DFT/MRCI picture, the ICT character of the primary donor state ($2A_g$) appears to be transient.[39] What we can safely state is that both $1B_u$ and $2A_g$ can exhibit ICT character (geometry-dependent), in agreement with previous results.[12e, 12f, 17b] When taking into account previous DFT/MRCI data on BLA and ICT,[17b] we conclude that the ground-state geometry is on the higher end of the possible BLA range. To preserve high ICT character, the $2A_g$ minimum would therefore need to exhibit a similar or higher BLA as the ground-state geometry. Considering the MNDO/CAS-CI results from Bricker and Lo,[16e] their $2A_g$ gas-phase minimum apparently has a lower BLA than the $1A_g$ minimum but a higher BLA than the $1B_u$ minimum (no explicit are values given). This matches the experimental assessment of the donor state being of partially both LE and ICT character.[41] As already mentioned above, the BLA is less pronounced at the CIS[8,8] ICT minimum geometry[12e, 12f] than at the corresponding TD-CAM-B3LYP geometry, which may explain the differences in the calculated state energies at the ICT minimum geometry.

Our own computed dipole moments in the gas phase are quite similar to those calculated at the QM/MM level without surrounding point charges (with a maximum difference of 1.5 D). Upon activation of the MM point charges, we see a drastic increase in the QM/MM dipole moment of each state (roughly doubled). The relocation of charge is thus favored by the protein environment, which apparently stabilizes the ICT states. This is reflected in the relative absorption energies, as will be seen below (Table 3).

(d) Spectral influence of the protein

In section (b), we have discussed the computed state energies of Per and Chl *a* in the gas phase and in acetone solution. In PCP, the environment of the chromophore apparently favors ICT (see Table 2 and Ref. 12f) so that one may expect changes in the absorption energies of the LE or ICT states relative to

**Table 3. Vertical excitation energies ($\Delta E_v$, in eV) and oscillator strengths (f) of Chl *a* and Per, from TD-CAM-B3LYP and DFT/MRCI calculations at the QM/MM ground-state minimum, with and without the PCP point charges. Average values over five QM/MM snapshots are given for Per, standard deviations are not listed (for $\Delta E_v$: 0.03 eV or smaller, for f: 0.06 or smaller).**

| | Gas Phase, QM/MM geom | | | | Point charge field, QM/MM geom | | | |
|---|---|---|---|---|---|---|---|---|
| | TD-DFT | | DFT/MRCI | | TD-DFT | | DFT/MRCI | |
| | $\Delta E_v$ | f | $\Delta E_v$ | f | $\Delta E_v$ | f | $\Delta E_v$ | f |
| $Q_y$ | 2.12 | 0.21 | 1.97 | 0.26 | 2.12 | 0.22 | 1.96 | 0.29 |
| $Q_x$ | 2.42 | 0.05 | 2.13 | 0.04 | 2.43 | 0.06 | 2.12 | 0.05 |
| Soret1 | 3.38 | 0.55 | 3.04 | 0.35 | 3.49 | 0.53 | 3.04 | 0.35 |
| Soret2 | 3.56 | 0.32 | 3.02 | 0.47 | 3.63 | 0.69 | 2.98 | 0.46 |
| $2A_g$ | / | / | 2.48 | 1.00 | / | / | 2.33 | 2.02 |
| $1B_u$ | 2.85 | 3.54 | 2.73 | 2.40 | 2.71 | 3.45 | 2.76 | 1.31 |
| $2B_u$ | / | / | 3.33 | 0.01 | / | / | 3.35 | 0.00 |

each other. We have examined these issues only at the QM/MM ground-state geometries, since QM/MM excited-state optimizations are still very costly.

Upon introduction of the protein environment in the form of point charges, there are only rather slight changes in the absorption patterns. The corresponding data are collected in Table 3. An experimental spectrum is shown in Figure 1 for comparison.

The experimental spectrum of PCP exhibits a large peak around 2.6 eV, which originates almost exclusively from Per, while Chl *a* contributes the Soret sub-peak at 2.9 eV and the Q band at 1.9 eV. As indicated by our gas phase and PCM calculations, as well as several other thorough studies,[16f, 12e, 12f, 16e] there is a significant and even dominant contribution from the $2A_g$ state to the computed absorption spectrum. Compared to other carotenoids,[12d] Per closes the energy gap between $1B_u$ and $2A_g$, which leads to a sharing of oscillator strength between these states. The physical origins of this effect were elucidated by Knecht et al.[16f] They can be traced to a redistribution of the HOMO → LUMO single excitation between these states, which in turn can be related to the molecular structure of Per.

These results are in slight disagreement with recent work by Bricker and Lo,[16e] who assigned $1B_u$ of the investigated Per (PID614) to carry the main bulk of transition dipole moment, as with most of their Per molecules. However, they observe some cases of oscillator strength redistribution as well. These differences probably arise from differences in the molecular geometries and the employed theoretical methods. The physical meaning of the results is however identical: Per appears to be able to provide $2A_g$ with oscillator strength, a feature that actually has already been experimentally observed.[43] However, the role of this absorption was so far considered to be minute compared to the absorption of $1B_u$, and also not of much practical importance

as $1B_u$ population would form a common pool with $2A_g$ by internal conversion from $1B_u$ to $2A_g$.

Coming back to our results in Table 3, it appears that the protein environment governs the fine tuning of oscillator strength distribution between $1A_g \rightarrow 1B_u$ and $1A_g \rightarrow 2A_g$. We have tested a small variety of different implicit environments for Per and find that the PCP point charge distribution delivers the strongest oscillator strength for the $1A_g \rightarrow 2A_g$ transition (2.02), compared to the oscillator strengths in acetone (1.69) and water (1.70, data not included in Table 1 or Table 2). The $f(2A_g)$ value in the protein even exceeds the theoretical maximum of oscillator strength predicted for the gas-phase and acetonitrile cases, which is just below 2.0 at high BLA values.[16f] It is further intriguing that this appears to be largely independent of the dynamic fluctuations in the protein, as the root-mean-square deviations of the oscillator strengths between snapshots are 0.06 or less (data not shown).

Judging from our model, the protein environment specifically increases the oscillator strength of the $2A_g$ state, but not at the cost of the "green" absorption energy, which would be diminished by closing the gap between $2A_g$ and $1B_u$. Instead, the gap is increased from 0.25 eV in the gas phase to 0.43 eV in the point charge field. Given that the protein environment stabilizes ICT states (see Table 2), the specific stabilization of $2A_g$ upon including the point charges makes sense. It thus appears that the price paid for mixing HOMO → LUMO contributions into the $1A_g \rightarrow 2A_g$ absorption, namely a blue shift of $2A_g$, is reduced by subsequent specific stabilization of ICT character by the protein environment.

(e) Dipole-dipole coupling

To assess the interaction between Chl *a* and Per, it is important to judge the potential coupling on the basis of the transition dipole moments.[44] This will allow us to understand how likely the individual states are to mix or exchange population upon approaching degeneracy.

We restrict ourselves here to an analysis of the collinearity between transition dipoles, for reasons outlined elsewhere.[17c, 17d] We compute the collinearity c (in percent) between two transitions to states n and m from

$$c = |\theta(\boldsymbol{\mu}_{0n}, \boldsymbol{\mu}_{0m})-(\pi/2)| \,/\, (\pi/2) \qquad (2)$$

with θ representing the angle between the two transition dipole vectors **μ**, which are located on different molecules. The corresponding results are shown in Table 4, as averages over five snapshots.

**Table 4. Collinearities (in %) between the transition dipole moments of the given states of Chl *a* (rows) vs. Per (columns) and the corresponding standard deviations, calculated for TD-CAM-B3LYP and DFT/MRCI at the QM/MM ground-state minimum, with and without the PCP point charges.**

| | Gas Phase | | | |
|---|---|---|---|---|
| | TD-DFT | DFT/MRCI | | |
| | $1B_u$ | $2A_g$ | $1B_u$ | $2B_u$ |
| $Q_y$ | 88.2 ± 0.2 | 86.3 ± 0.3 | 85.9 ± 0.1 | 83.6 ± 0.5 |
| $Q_x$ | 35.0 ± 0.1 | 7.3 ± 0.1 | 6.5 ± 0.2 | 5.8 ± 0.4 |
| Soret1 | 6.5 ± 0.2 | 8.7 ± 0.1 | 7.9 ± 0.2 | 7.1 ± 0.4 |
| Soret2 | 28.2 ± 0.1 | 83.4 ± 0.1 | 84.7 ± 0.2 | 84.4 ± 0.6 |
| | Point charge field | | | |
| | TD-DFT | DFT/MRCI | | |
| | $1B_u$ | $2A_g$ | $1B_u$ | $2B_u$ |
| $Q_y$ | 87.1 ± 0.1 | 85.1 ± 0.3 | 84.0 ± 0.2 | 78.2 ± 2.7 |
| $Q_x$ | 37.0 ± 0.1 | 0.4 ± 0.1 | 1.7 ± 0.2 | 8.5 ± 5.1 |
| Soret1 | 18.5 ± 0.1 | 24.3 ± 0.1 | 25.6 ± 0.2 | 15.0 ± 5.1 |
| Soret2 | 82.7 ± 0.2 | 60.5 ± 0.2 | 59.3 ± 0.2 | 67.4 ± 4.4 |

The highest collinearities are found for $Q_y$, exhibiting c values close to 80% or higher for almost all Per states in all environments. As $Q_y$ is the target for energy transfer, this is not surprising. Thus, our simple coupling model agrees with the experimental evidence of a strong energy transfer from Per to $Q_y$.[9] Interestingly, the coupling to $Q_y$ does not discriminate between the Per states. High c values are found even for the $2B_u$ state, which is definitely not involved in the energy transfer pathway. As the high c values for $Q_y$ are independent of the presence of point charges, we conclude that it is the spatial orientation of the investigated Per and Chl *a* that leads to the high collinearities.

For the other states, TD-DFT and DFT/MRCI disagree to some extent: TD-DFT shows a slight collinearity of $1B_u$ to $Q_x$ and Soret2, which is significantly increased for Soret2 upon activation of the point charges (from 28% to 83%). DFT/MRCI, on the other hand, predicts no collinearity at all to $Q_x$, as well as only weak coupling to Soret1 in the gas phase; instead, Soret2 shows a strong collinearity (> 83%) to all Per states. Upon introduction of the point charges, DFT/MRCI shows reduced coupling of all Per states to Soret2 (e.g., collinearity drops from 85% to 59% for Soret2/$1B_u$), whereas the coupling of Soret1 to the Per states is more than doubled (e.g., collinearity rises from 8% to 26% for Soret1/$1B_u$).

Regardless of the choice of DFT/MRCI or TD-DFT, the picture resulting from the introduction of the point charges is consistent for both methods: It is not only the Q-band that couples to the Per states, but there may also a coupling to the Soret states. This coupling scheme has been reported previously for xanthophylls.[17c, 17d] However, one has to remember that PCP only contains two Chl *a* compared to eight Per; excitation of the Chl *a* Soret states will thus occur only rarely in the spectral region featuring absorption both to the Soret and $1B_u$ states.

## Summary and discussion

We have investigated the effect of the protein environment on the electronic states of a Per/Chl *a* pair from the PCP complex and the consequences for the energy transfer mechanism. We find that the protein supports the formation of states with ICT character. Furthermore, in agreement with the results from earlier studies, there is significant ICT character in the excited singlet states of Per,[12e, 12f, 16e, 16f] depending on the BLA of the given geometry. The energy of the $1B_u$ state drops drastically upon geometry relaxation, in agreement with our earlier studies on other carotenoids and Per.[12d-f, 17d] Considering the ICT-stabilizing protein environment and the insights on the $2A_g$ state from earlier

work, we arrive at a new picture for Per → Chl *a* energy transfer which might resolve the ICT/LE ambiguity of the Per donor state.[9, 39, 41] This picture is similar to that presented by Wagner et al.,[12f] especially in terms of the $1B_u$ state acquiring ICT character upon geometry relaxation, but differs in crucial points concerning initial excitation, state crossings, and donor state order.

Our current model proposes that after vertical excitation, the $1B_u$ state undergoes very fast geometrical relaxation (rather than internal conversion) to reach fluorescence regions close to $2A_g$. This is consistent with earlier notions[12f] and supported by the data in Table 1, which show that the vertical fluorescence energy of the relaxed $1B_u$ state is 2.31 eV, about 0.2 eV lower than the vertical absorption energy of $2A_g$ upon excitation at the ground-state minimum geometry. As $1B_u$ takes on ICT character upon relaxation, the protein environment can be expected to lower the $1B_u$ emission even further. This leads to the simplified qualitative state energy diagram shown in Figure 4 (right side).

Note that the proposed model does not invoke an IC between $1B_u$ and $2A_g$, a scenario that has so far not been considered. The main difference to the commonly accepted models is that we expect $1B_u$ to act directly as an energy donor to Chl *a*, as already indicated by several experiments.[13, 39, 42] For such an "$S_2$ pathway", the orientation of the DFT/MRCI transition dipoles (Table 4) appears to be more beneficial for non-adiabatic coupling between $1B_u$ and $Q_y$ than for energy transfer from $1B_u$ to hot $Q_x$ states of Chl *a.*[13, 42] Furthermore, our calculations indicate that fast geometry relaxation of the $1B_u$ state of Per induces ICT character and lowers the energy sufficiently to facilitate direct energy transfer to the $Q_y$ state of Chl *a*. Relaxation of $2A_g$, Figure 4 (left side), will presumably reach a different minimum (not computed) that might even be below the $1B_u$ ICT minimum. There is no need for a population transfer between $1B_u$ and $2A_g$ as both states appear to be strongly absorbing when in the protein environment; we also find no crossings with $2A_g$ along the $1B_u$ relaxation path contrary to earlier calculations.[12f] A very recent peridinin 2D-IR study shows that different transient IR relaxation profiles occur depending on the UV/vis excitation wave length.[45]

Our simple dipole coupling scheme (Table 4) does not indicate any preference for $2A_g$ as donating Per state over $1B_u$. It might actually be very difficult to distinguish between a fluorescence signal from $1B_u$ and $2A_g$, especially since they apparently change their character (LE/ICT) upon relaxation and end up in similar spectral regions with a large difference between absorption and emission energy (~0.4-0.5 eV).

With this in mind, we propose that the spectroscopic signals attributed to the much sought-after $S_1$/ICT state can probably be attributed to the relaxed $1B_u$ state (ICT at minimum) and the relaxed $2A_g$ state (likely LE or mixed LE/ICT

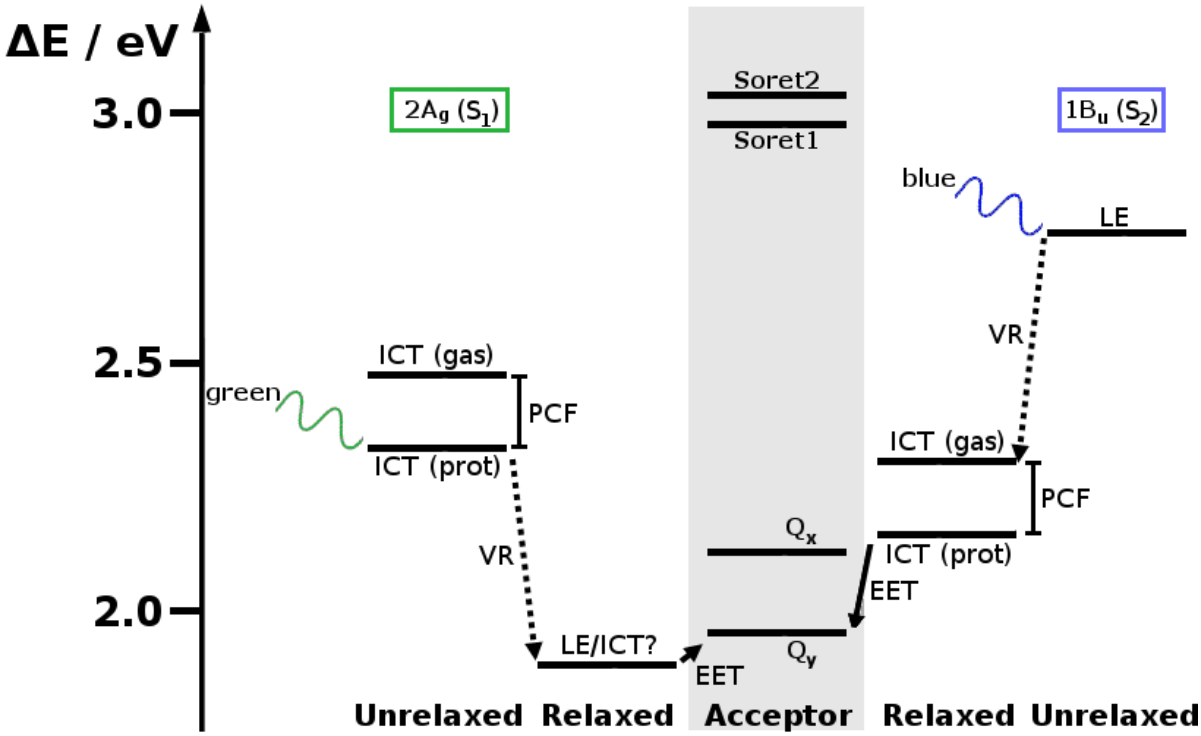


**Figure 4.** Proposed Per → Chl *a* energy transfer scheme based on DFT/MRCI calculations at the QM/MM geometries along with the gas-phase data for $1B_u$ relaxation. The energy associated with vibrational relaxation (VR) of the $2A_g$ state is taken from Bricker and Lo (MNDO/CAS-CI).[16e] The effect of the PCF on ICT states is assumed to be the same for $2A_g$ and $1B_u$. The $2A_g$ minimum character (LE/ICT) is unknown.

character, judging from the data presented elsewhere[12e, 12f, 16f]). The low energy of the relaxed $1B_u$ state allows for direct energy transfer to the $Q_y$ state, as supported by our dipole model (rather than donation to Chl *a* via $Q_x$).

There are distinct advantages to this model: The pathways resulting from the $1B_u$ state are indeed the only ones available for PCP reconstituted with Chl *b*, which has a Q band that is slightly higher in energy than that of Chl *a*. Consequently, in the Chl *b*-PCP constructs, $2A_g$ is apparently too low in energy to still donate efficiently to $Q_y$.[46] Experimentally, a larger time constant was established for the energy transfer to Chl *b* compared to other Chls,[46b] while the actual loss in EET efficiency is only 55%.[46a] If the ICT state would be the lowest donating state, and the final relaxation point for both initially populated states (as proposed[12f]) one would expect a near-100% loss of EET efficiency. Judging from the proposed IC and EET times of 100-150 fs,[9] we consider our model to be a sound alternative: The core difference is that we do without IC between $1B_u$ and $2A_g$ by invoking vibrational relaxation and EET. From our calculations and the work by Knecht et al.,[16f] it appears that $2A_g$ receives its own share of population by direct excitation; the almost 50/50 distribution of oscillator strengths between $1A_g \rightarrow 2A_g$ and $1A_g \rightarrow 1B_u$ would explain why about 50% of the irradiated energy is lost when having Chl *b* as acceptor chromophore. We emphasize that other theoretical studies have also found

significant oscillator strength for the $1A_g \rightarrow 2A_g$ transition.[16f, 16h] In our model, we observe no state crossings along the $1B_u$ relaxation path (the state order is conserved at the $1B_u$ minimum, Table 1), and hence there is no obvious way for the $1B_u$ population to convert quickly into $2A_g$ population or vice versa. Still, for a complete model, one needs to address the influence of the other chromophores, such as the other Per molecules in PCP, as has been done recently.[16g]

A potential concern about our proposed model is the required sub-ps time scale for excited-state geometry relaxation. It is however well known from experiments and from excited-state dynamics simulations on other systems that photoinduced geometry changes can indeed be ultrafast (sub-ps), especially when they involve a steep downhill motion from the Franck-Condon region.[47] In the present case, the optimized Per structures change only slightly along the conjugated chain when going from the ground state to the excited $B_u$ state; an analysis for the gas phase can be found in the SI. The required atomic repositioning is quite small (less than 0.05 Å for the core part of the chain, see SI), hence we expect that the associated downhill relaxation is very fast. Comparing to the spectral components from experiment,[13] we can tentatively assign our proposed relaxation channels to the 0.7 ps ($1B_u$) and the 3 ps components ($2A_g$). The ultrafast (<100 fs) non-adiabatic channel is not covered by our calculations, but may result from hot $1B_u$ states coupling to $Q_y$.

To conclude, our proposed model attempts to reconcile several aspects of earlier theoretical and experimental work in order to arrive at a consistent scenario. This is done on the basis of two theoretical findings in the present work and in other recent computational studies on peridinine:[16e-g] (i) The gain in oscillator strength of the $2A_g$ state allowing for direct excitation, and (ii) the strong drop in the $1B_u$ energy upon geometrical relaxation while retaining the order of states. Our model puts these two findings into the context of the experimental literature – by invoking fast vibrational relaxation rather than internal conversion as dominant feature in the energy transfer mechanism.

**Acknowledgments**

JPG is grateful to Dr. habil. Heiko Lokstein for providing the experimental spectrum of PCP in water and for many helpful discussions.

## References


1. Prezelin, B. B.; Haxo, F. T., Purification and characterization of peridinin-chlorophyll a-proteins from marine dinoflagellates Glenodinium sp and Gonyaulax polyedra. *Planta* **1976,** *128* (2), 133-141.

2. (a) Akimoto, S.; Takaichi, S.; Ogata, T.; Nishimura, Y.; Yamazaki, I.; Mimuro, M., Excitation energy transfer in carotenoid-chlorophyll protein complexes probed by femtosecond fluorescence decays. *Chem. Phys. Lett.* **1996,** *260* (1-2), 147-152; (b) Kleima, F. J.; Wendling, M.; Hofmann, E.; Peterman, E. J. G.; van Grondelle, R.; van Amerongen, H., Peridinin chlorophyll a protein: Relating structure and steady-state spectroscopy. *Biochemistry* **2000,** *39* (17), 5184-5195.

3. Strain, H. H.; Svec, W. A.; Aitzetmüller, K.; Grandolfo, M. C.; Katz, J. J.; Kjøsen, H.; Norgård, S.; Liaaen-Jensen, S.; Haxo, F. T.; Wegfahrt, P.; Rapoport, H., Structure of peridinin, characteristic dinoflagellate carotenoid. *J. Am. Chem. Soc.* **1971,** *93* (7), 1823-1825.

4. Hofmann, E.; Wrench, P. M.; Sharples, F. P.; Hiller, R. G.; Welte, W.; Diederichs, K., Structural basis of light harvesting by carotenoids: Peridinin-chlorophyll-protein from Amphidinium carterae. *Science* **1996,** *272* (5269), 1788-1791.

5. Schulte, T.; Sharples, F. P.; Hiller, R. G.; Hofmann, E., X-ray Structure of the High-Salt Form of the Peridinin-Chlorophyll a-Protein from the Dinoflagellate Amphidinium carterae: Modulation of the Spectral Properties of Pigments by the Protein Environment. *Biochemistry* **2009,** *48* (21), 4466-4475.

6. Scholes, G. D.; Fleming, G. R.; Olaya-Castro, A.; van Grondelle, R., Lessons from nature about solar light harvesting. *Nature Chemistry* **2011,** *3* (10), 763-774.

7. (a) Yoon, H. S.; Hackett, J. D.; Bhattacharya, D., A single origin of the peridinin- and fucoxanthin-containing plastids in dinoflagellates through tertiary endosymbiosis. *Proc. Natl. Acad. Sci.* **2002,** *99* (18), 11724-11729; (b) Polívka, T.; Sundström, V., Ultrafast dynamics of carotenoid excited States-from solution to natural and artificial systems. *Chem. Rev.* **2004,** *104* (4), 2021-2071.

8. Song, P. S.; Koka, P.; Prezelin, B. B.; Haxo, F. T., Molecular topology of photosynthetic light-harvesting pigment complex, peridinin-chlorophyll a-protein, from marine dinoflagellates. *Biochemistry* **1976,** *15* (20), 4422-4427.

9. Polívka, T.; Hofmann, E., Structure-Function Relationship in Peridinin-Chlorophyll Proteins. In *Structural Basis of Biological Energy Generation*, Hohmann-Marriott, M. F., Ed. Springer: Dordrecht, 2014; Vol. 39, pp 39-58.

10. Pariser, R., Theory of the electronic spectra and structure of the polyacenes and of alternant hydrocarbons. *J. Chem. Phys.* **1956,** *24* (2), 250-268.

11. Kleinschmidt, M.; Marian, C. M.; Waletzke, M.; Grimme, S., Parallel multireference configuration interaction calculations on mini- $\beta$ -carotenes and $\beta$-carotene. *J. Chem. Phys.* **2009,** *130* (4), 044708.

12. (a) Siefermann-Harms, D., Carotenoids in photosynthesis .1. Location in photosynthetic membranes and light-harvesting function. *Biochim. Biophys. Acta* **1985,** *811* (4), 325-355; (b) Frank, H. A.; Cua, A.; Chynwat, V.; Young, A.; Gosztola, D.; Wasielewski, M. R., Photophysics of the carotenoids associated with the xanthophyll cycle in photosynthesis. *Photosynth. Res.* **1994,** *41*, 389-395; (c) Starcke, J. H.; Wormit, M.; Schirmer, J.; Dreuw, A., How much double excitation character do the lowest excited states of linear polyenes have? *Chem. Phys.* **2006,**

*329*, 39-49; (d) Götze, J. P.; Thiel, W., TD-DFT and DFT/MRCI study of electronic excitations in Violaxanthin and Zeaxanthin. *Chem. Phys.* **2013,** *415*, 247-255; (e) Enriquez, M. M.; Fuciman, M.; LaFountain, A. M.; Wagner, N. L.; Birge, R. R.; Frank, H. A., The Intramolecular Charge Transfer State in Carbonyl-Containing Polyenes and Carotenoids. *J. Phys. Chem. B* **2010,** *114* (38), 12416-12426; (f) Wagner, N. L.; Greco, J. A.; Enriquez, M. M.; Frank, H. A.; Birge, R. R., The Nature of the Intramolecular Charge Transfer State in Peridinin. *Biophys. J.* **2013,** *104* (6), 1314-1325.

13. Zigmantas, D.; Hiller, R. G.; Sundstrom, V.; Polivka, T., Carotenoid to chlorophyll energy transfer in the peridinin-chlorophyll-a-protein complex involves an intramolecular charge transfer state. *Proc. Natl. Acad. Sci.* **2002,** *99* (26), 16760-16765.

14. (a) Jamorski, C.; Casida, M. E.; Salahub, D. R., Dynamic polarizabilities and excitation spectra from a molecular implementation of time-dependent density-functional response theory: N-2 as a case study. *J. Chem. Phys.* **1996,** *104*, 5134-5147; (b) Casida, M. E.; Jamorski, C.; Casida, K. C.; Salahub, D. R., Molecular excitation energies to high-lying bound states from time-dependent density-functional response theory: Characterization and correction of the time-dependent local density approximation ionization threshold. *J. Chem. Phys.* **1998,** *108* (11), 4439-4449.

15. Mikhailov, I.; Tafur, S.; Masunov, A. E., Double excitations and state-to-state transition dipoles in $\pi-\pi$ excited singlet states of linear polyenes: Time-dependent density-functional theory versus multiconfigurational methods. *Phys. Rev. A* **2008,** *77* (1), 012510.

16. (a) Dreuw, A.; Starcke, J. H.; Wachtveitl, J., Excited state properties of the astaxanthin radical cation: A quantum chemical study. *Chem. Phys.* **2010,** *373* (1-2), 2-7; (b) Damjanovic, A.; Ritz, T.; Schulten, K., Excitation transfer in the peridinin-chlorophyll-protein of Amphidinium carterae. *Biophys. J.* **2000,** *79* (4), 1695-1705; (c) Duffy, C. D. P.; Ruban, A. V.; Barford, W., Theoretical investigation of the role of strongly coupled chlorophyll dimers in photoprotection of LHCII. *J. Phys. Chem. B* **2008,** *112*, 12508-12515; (d) Duffy, C. D. P.; Valkunas, L.; Ruban, A. V., Quantum Mechanical Calculations of Xanthophyll-Chlorophyll Electronic Coupling in the Light-Harvesting Antenna of Photosystem II of Higher Plants. *J. Phys. Chem. B* **2013,** *117* (25), 7605-7614; (e) Bricker, W. P.; Lo, C. S., Excitation Energy Transfer in the Peridinin-Chlorophyll a-Protein Complex Modeled Using Configuration Interaction. *J. Phys. Chem. B* **2014,** *118* (31), 9141-9154; (f) Knecht, S.; Marian, C. M.; Kongsted, J.; Mennucci, B., On the Photophysics of Carotenoids: A Multireference DFT Study of Peridinin. *J. Phys. Chem. B* **2013,** *117* (44), 13808-13815; (g) Andreussi, O.; Knecht, S.; Marian, C. M.; Kongsted, J.; Mennucci, B., Carotenoids and Light-Harvesting: From DFT/MRCI to the Tamm-Dancoff Approximation. *J. Chem. Theory Comput.* **2015,** *11* (2), 655-666; (h) Coccia, E.; Varsano, D.; Guidoni, L., Ab Initio Geometry and Bright Excitation of Carotenoids: Quantum Monte Carlo and Many Body Green's Function Theory Calculations on Peridinin. *J. Chem. Theory Comput.* **2014,** *10* (2), 501-506; (i) Starcke, J. H.; Wormit, M.; Dreuw, A., Nature of the lowest excited states of neutral polyenyl radicals and polyene radical cations. *J. Chem. Phys.* **2009,** *131* (14), 144311.

17. (a) Limacher, P. A.; Mikkelsen, K. V.; Lüthi, H. P., On the accurate calculation of polarizabilities and second hyperpolarizabilities of polyacetylene oligomer chains using the CAM-B3LYP density functional *J. Chem. Phys.* **2009,** *130*, 194114; (b) Klaumünzer, B.; Kröner, D.; Saalfrank, P., (TD-)DFT Calculation of Vibrational and Vibronic Spectra of Riboflavin in Solution. *J. Phys. Chem. B* **2010,** *114* (33), 10826-10834; (c) Kröner, D.; Götze, J. P., Modeling of a violaxanthin-chlorophyll b chromophore pair in its LHCII environment using CAM-B3LYP. *J. Photochem. Photobiol. B* **2012,** *109*, 12-19; (d) Götze, J. P.; Kröner, D.; Banerjee, S.; Karasulu,

B.; Thiel, W., Carotenoids as a Shortcut for Chlorophyll Soret-to-Q Band Energy Flow. *ChemPhysChem* **2014,** *15* (15), 3392-3401.
18. (a) Shima, S.; Ilagan, R. P.; Gillespie, N.; Sommer, B. J.; Hiller, R. G.; Sharples, F. P.; Frank, H. A.; Birge, R. R., Two-photon and fluorescence spectroscopy and the effect of environment on the photochemical properties of peridinin in solution and in the peridinin-chlorophyll-protein from Amphidinium carterae. *J. Phys. Chem. A* **2003,** *107* (40), 8052-8066; (b) Ilagan, R. P.; Koscielecki, J. F.; Hiller, R. G.; Sharples, F. P.; Gibson, G. N.; Birge, R. R.; Frank, H. A., Femtosecond time-resolved absorption spectroscopy of main-form and high-salt peridinin-chlorophyll a-proteins at low temperatures. *Biochemistry* **2006,** *45* (47), 14052-14063.
19. (a) Sherwood, P.; de Vries, A. H.; Guest, M. F.; Schreckenbach, G.; Catlow, C. R. A.; French, S. A.; Sokol, A. A.; Bromley, S. T.; Thiel, W.; Turner, A. J.; Billeter, S.; Terstegen, F.; Thiel, S.; Kendrick, J.; Rogers, S. C.; Casci, J.; Watson, M.; King, F.; Karlsen, E.; Sjovoll, M.; Fahmi, A.; Schafer, A.; Lennartz, C., QUASI: A general purpose implementation of the QM/MM approach and its application to problems in catalysis. *Theochem-J. Mol. Struct.* **2003,** *632*, 1-28; (b) Senn, H. M.; Thiel, W., QM/MM methods for Biomolecular Systems. *Angew. Chem.-Int. Edit.* **2009,** *48* (7), 1198-1229.
20. Brooks, B. R.; Brooks, C. L.; Mackerell, A. D.; Nilsson, L.; Petrella, R. J.; Roux, B.; Won, Y.; Archontis, G.; Bartels, C.; Boresch, S.; Caflisch, A.; Caves, L.; Cui, Q.; Dinner, A. R.; Feig, M.; Fischer, S.; Gao, J.; Hodoscek, M.; Im, W.; Kuczera, K.; Lazaridis, T.; Ma, J.; Ovchinnikov, V.; Paci, E.; Pastor, R. W.; Post, C. B.; Pu, J. Z.; Schaefer, M.; Tidor, B.; Venable, R. M.; Woodcock, H. L.; Wu, X.; Yang, W.; York, D. M.; Karplus, M., CHARMM: The Biomolecular Simulation Program. *J. Comp. Chem.* **2009,** *30* (10), 1545-1614.
21. Ryckaert, J. P.; Ciccotti, G.; Berendsen, H. J. C., Numerical-integration of Cartesian equations of motion of a system with constraints - Molecular-dynamics of n-alkanes. *J. Comput. Phys.* **1977,** *23* (3), 327-341.
22. (a) Nosé, S., A unified formulation of the constant temperature molecular-dynamics methods. *J. Chem. Phys.* **1984,** *81* (1), 511-519; (b) Hoover, W. G., Canonical dynamics - equilibrium phase-space distributions. *Phys. Rev. A* **1985,** *31* (3), 1695-1697.
23. Karasulu, B.; Patil, M.; Thiel, W., Amine Oxidation Mediated by Lysine-Specific Demethylase 1: Quantum Mechanics/Molecular Mechanics Insights into Mechanism and Role of Lysine 661. *J. Am. Chem. Soc.* **2013,** *135* (36), 13400-13413.
24. Besler, B. H.; Merz Jr., K. M.; Kollman, P. A., Atomic charges derived from semiempirical methods. *J. Comp. Chem.* **1990,** *11*, 431-439.
25. (a) Becke, A. D., Density-functional thermochemistry .3. The role of exact exchange. *J. Chem. Phys.* **1993,** *98*, 5648-5652; (b) Lee, C.; Yang, W.; Parr, R. G., Development of the Colle-Salvetti correlation-energy formula into a functional of the electron-density. *Phys. Rev. B* **1988,** *37*, 785-789.
26. Hariharan, P. C.; Pople, J. A., Influence of polarization functions on molecular-orbital hydrogenation energies. *Theor. Chim. Acta* **1973,** *28* (3), 213-222.
27. Dewar, M. J. S.; Thiel, W., Ground-states of Molecules .38. MNDO Method - Approximations and Parameters. *J. Am. Chem. Soc.* **1977,** *99* (15), 4899-4907.
28. Frisch, M. J.; Trucks, G. W.; Schlegel, H. B.; Scuseria, G. E.; Robb, M. A.; Cheeseman, J. R.; Scalmani, G.; Barone, V.; Mennucci, B.; Petersson, G. A.; Nakatsuji, H.; Caricato, M.; Li, X.; Hratchian, H. P.; Izmaylov, A. F.; Bloino, J.; Zheng, G.; Sonnenberg, J. L.; Hada, M.; Ehara, M.; Toyota, K.; Fukuda, R.; Hasegawa, J.; Ishida, M.; Nakajima, T.; Honda, Y.; Kitao, O.; Nakai, H.; Vreven, T.; J. A. Montgomery, J.; Peralta, J. E.; Ogliaro, F.; Bearpark, M.; Heyd, J. J.;

Brothers, E.; Kudin, K. N.; Staroverov, V. N.; Keith, T.; Kobayashi, R.; Normand, J.; Raghavachari, K.; Rendell, A.; Burant, J. C.; Iyengar, S. S.; Tomasi, J.; Cossi, M.; Rega, N.; Millam, J. M.; Klene, M.; Knox, J. E.; Cross, J. B.; Bakken, V.; Adamo, C.; Jaramillo, J.; Gomperts, R.; Stratmann, R. E.; Yazyev, O.; Austin, A. J.; Cammi, R.; Pomelli, C.; Ochterski, J. W.; Martin, R. L.; Morokuma, K.; Zakrzewski, V. G.; Voth, G. A.; Salvador, P.; Dannenberg, J. J.; Dapprich, S.; Daniels, A. D.; Farkas, O.; Foresman, J. B.; Ortiz, J. V.; Cioslowski, J.; Fox, D. J., Gaussian 09, Revision B.01. *Gaussian 09, Revision B.01, Gaussian, Inc., Wallingford CT* **2010**.

29. Smith, W.; Yong, C. W.; Rodger, P. M., DL_POLY: Application to molecular simulation. *Mol. Simul.* **2002,** *28* (5), 385-471.

30. Yanai, T.; Tew, D.; Handy, N., A new hybrid exchange-correlation functional using the Coulomb-attenuating method (CAM-B3LYP). *Chem. Phys. Lett.* **2004,** *393* (1-3), 51-57.

31. (a) Barone, V.; Cossi, M., Quantum calculation of molecular energies and energy gradients in solution by a conductor solvent model. *J. Phys. Chem. A* **1998,** *102* (11), 1995-2001; (b) Cossi, M.; Rega, N.; Scalmani, G.; Barone, V., Energies, structures, and electronic properties of molecules in solution with the C-PCM solvation model. *J. Comp. Chem.* **2003,** *24* (6), 669-681.

32. Schäfer, A.; Klamt, A.; Sattel, D.; Lohrenz, J. C. W.; Eckert, F., COSMO Implementation in TURBOMOLE: Extension of an efficient quantum chemical code towards liquid systems. *Phys. Chem. Chem. Phys.* **2000,** *2* (10), 2187-2193.

33. Grimme, S.; Waletzke, M., A combination of Kohn-Sham density functional theory and multi-reference configuration interaction methods. *J. Chem. Phys.* **1999,** *111* (13), 5645-5655.

34. Ahlrichs, R., TURBOMOLE V6.1, a development of University of Karlsruhe and Forschungszentrum Karlsruhe GmbH, 1989-2007, TURBOMOLE GmbH, since 2007; available from http://www.turbomole.com.

35. Becke, A. D., A new mixing of Hartree-Fock and local density-functional theories. *J. Chem. Phys.* **1993,** *98* (2), 1372-1377.

36. Schäfer, A.; Horn, H.; Ahlrichs, R., Fully optimized contracted Gaussian-basis sets for atoms Li to Kr. *J. Chem. Phys.* **1992,** *97* (4), 2571-2577.

37. Senge, M. O.; Hope, H.; Smith, K. M., Structure and conformation of photosynthetic pigments and related compounds. 3. Crystal structure of β-carotene. *Z. Naturforsch. C* **1992,** *47* (5-6), 474-476.

38. Strain, H. H.; Thomas, M. R.; Katz, J. J., Spectral absorption properties of ordinary and fully deuterated chlorophylls alpha and beta. *Biochim. Biophys. Acta* **1963,** *75* (3), 306-311.

39. Krueger, B. P.; Lampoura, S. S.; van Stokkum, I. H. M.; Papagiannakis, E.; Salverda, J. M.; Gradinaru, C. C.; Rutkauskas, D.; Hiller, R. G.; van Grondelle, R., Energy transfer in the peridinin chlorophyll-a protein of Amphidinium carterae studied by polarized transient absorption and target analysis. *Biophys. J.* **2001,** *80* (6), 2843-2855.

40. (a) Zigmantas, D.; Hiller, R. G.; Sharples, F. P.; Frank, H. A.; Sundstrom, V.; Polivka, T., Effect of a conjugated carbonyl group on the photophysical properties of carotenoids. *Phys. Chem. Chem. Phys.* **2004,** *6* (11), 3009-3016; (b) Polívka, T.; Pascher, T.; Hiller, R. G., Energy transfer in the peridinin-chicrophyll protein complex reconstituted with mixed chlorophyll sites. *Biophys. J.* **2008,** *94* (8), 3198-3207.

41. Bautista, J. A.; Connors, R. E.; Raju, B. B.; Hiller, R. G.; Sharples, F. P.; Gosztola, D.; Wasielewski, M. R.; Frank, H. A., Excited state properties of peridinin: Observation of a solvent dependence of the lowest excited singlet state lifetime and spectral behavior unique among

carotenoids. *J. Phys. Chem. B* **1999,** *103* (41), 8751-8758.
42. Linden, P. A.; Zimmermann, J.; Brixner, T.; Holt, N. E.; Vaswani, H. M.; Hiller, R. G.; Fleming, G. R., Transient absorption study of peridinin and peridinin-chlorophyll a-protein after two-photon excitation. *J. Phys. Chem. B* **2004,** *108* (29), 10340-10345.
43. Krikunova, M.; Lokstein, H.; Leupold, D.; Hiller, R. G.; Voigt, B., Pigment-pigment interactions in PCP of Amphidinium carterae investigated by nonlinear polarization spectroscopy in the frequency domain. *Biophys. J.* **2006,** *90* (1), 261-271.
44. Kasha, M.; Rawls, H. R.; Ashraf El-Bayoumi, M., Molecular spectroscopy. In *Eighth European Congress on Molecular Spectroscopy*, Butterworths, London, UK: Copenhagen, 1965; pp 371-392.
45. Di Donato, M.; Ragnoni, E.; Lapini, A.; Foggi, P.; Hiller, R. G.; Righini, R., Femtosecond transient infrared and stimulated Raman spectroscopy shed light on the relaxation mechanisms of photo-excited peridinin. *J. Chem. Phys.* **2015,** *142* (21), 10.
46. (a) Miller, D. J.; Catmull, J.; Puskeiler, R.; Tweedale, H.; Sharples, F. P.; Hiller, R. G., Reconstitution of the peridinin-chlorophyll a protein (PCP): Evidence for functional flexibility in chlorophyll binding. *Photosynth. Res.* **2005,** *86* (1-2), 229-240; (b) Polívka, T.; Pascher, T.; Sundstrom, V.; Hiller, R. G., Tuning energy transfer in the peridinin-chlorophyll complex by reconstitution with different chlorophylls. *Photosynth. Res.* **2005,** *86* (1-2), 217-227.
47. (a) Weingart, O.; Altoe, P.; Stenta, M.; Bottoni, A.; Orlandi, G.; Garavelli, M., Product formation in rhodopsin by fast hydrogen motions. *Phys. Chem. Chem. Phys.* **2011,** *13* (9), 3645-3648; (b) Polli, D.; Rivalta, I.; Nenov, A.; Weingart, O.; Garavelli, M.; Cerullo, G., Tracking the primary photoconversion events in rhodopsins by ultrafast optical spectroscopy. *Photochem. Photobiol. Sci.* **2015,** *14* (2), 213-228.

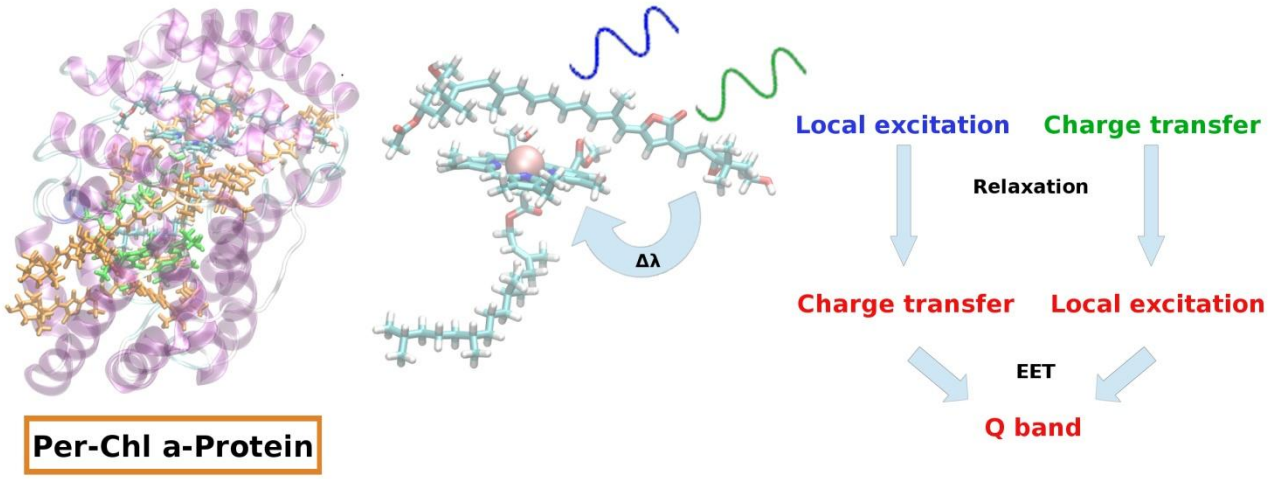


Graphical Abstract

## Highlights

- DFT/MM calculations on the peridinin–chlorophyll a–protein are reported.
- Strong relaxation after bright state excitation is observed.
- The energy transfer model involves a bright S1 state.
- Two parallel channels explain the efficiency loss upon chlorophyll exchange.